Electronic Supplementary Information

Ultraviolet Persistent Luminescence in Purely Organic Systems

Cong Liu,[1]* Yu Lang,[1] Jiadong Zhou,[1] Huiwen Zeng,[1] Xuan Zhang,[2] Qing Luo,[2] Bingjia Xu,[3] Guang Shi,[1] and Yujian Zhang[2]*

[1]*School of Chemistry, South China Normal University, Guangzhou 510006, PR China.*

[2]*Key Laboratory of the Ministry of Education for Advanced Catalysis Materials, Department of Chemistry, Zhejiang Normal University, Jinhua, 321004, P. R. China.*

[3]*School of Environmental and Chemical Engineering, Wuyi University, Jiangmen 529020, PR China.*

*Correspondence to: liucong011@163.com (C. L.); sciencezyj@foxmail.com; (Y. Z.)

Contents

Ⅰ. Experimental Section

Chemical Reagents and Materials

11,12-Dihydroindolo[2,3-A]carbazole (ICzO) was purchased from *MACKLIN*. 1,2-Dibromoethane, 1-bromoethane, melamine, formaldehyde aqueous solution, triethanolamine, 1,3-propylenediamine and polyvinyl alcohol (PVA, M.W. is 44050, Alcoholysis degree is 72.5-74.5%) were purchased from *Energy Chemical*. Bisphenol A diglycidyl ether (99%) was purchased from *Nippon Kayaku*. All of these chemical reagents were used as received. Other reagents and organic solvents were purchased from Guangzhou *Ruoyang* Company (China) with analytical grade and used without further purification.

Synthesis and Characterization

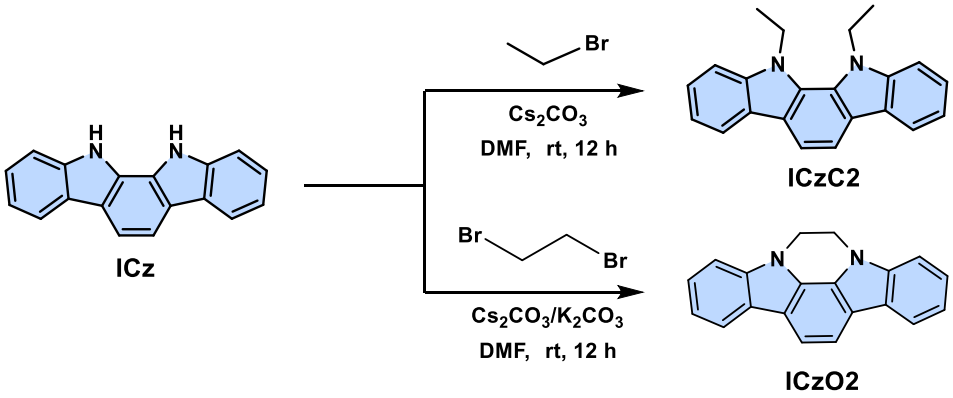

Scheme S1. Synthetic routes of **ICzO2** and **ICzC2**.

Synthesis of ICzC2: 11,12-dihydroindolo[2,3-A]carbazole (0.20 g, 0.78 mmol), bromoethane (0.21 g, 1.95 mmol) and cesium carbonate (0.64 g, 1.95 mmol) were added into 15 mL of DMF. Then the mixture was stirred at room temperature for 12 h. After the reaction was complete, the mixture was slowly poured into ice water with stirring and the yellowish product was precipitated. The crude product was isolated by suction filtration, washed with deionized water, and dried. Further, the crude product was purified by silica gel column chromatography with dichloromethane and petroleum ether (v/v=1:1) as eluent. The resulting solid was further recrystallized from dichloromethane/methanol to give a white solid powder. 11,12-diethyl-11,12-dihydroindolo[2,3-A]carbazole (ICzC2), white powder, yield 20.51% (0.05 g). ^{1}H NMR (600 MHz, Chloroform-*d*) δ = 8.13 (m, *J*=7.7, 1.0, 2H), 7.95 (s, 2H), 7.57 (d, *J*=8.1, 2H), 7.47 (m, *J*=8.2, 7.0, 1.2, 2H), 7.33-7.27 (m, 2H), 4.63 (q, *J*=7.1, 4H), 1.35 (t, *J*=7.2, 6H). ^{13}C NMR (151 MHz, $CDCl_3$) δ 143.24, 129.71, 126.25,

125.21, 124.58, 120.22, 119.89, 112.99, 111.15, 77.26, 77.04, 76.83, 43.00, 14.34. ESI-MS: m/z $[M+H]^+$ calculated for $C_{22}H_{21}N_2^+$: 313.16; found 313.17. HPLC: purity 99.9%.

Synthesis of ICzO2: According to the synthesis procedure of ICzC2, the white solid product was obtained from the compounds 11,12-dihydroindolo[2,3-A]carbazole (0.50 g, 1.95 mmol), 1,2-dibromoethane (0.81 g, 4.29 mmol) and potassium carbonate (0.59 g, 4.29 mmol). 4,4a,6,7-tetrahydrodiindolo[1,2,3-de:3',2',1'-ij]quinoxaline (ICzO2), white powder, yield 20.12% (0.11 g). ^{1}H NMR (600 MHz, $CDCl_3$) δ 8.14 (m, *J* = 7.9, 1.0 Hz, 2H), 7.79 (s, 2H), 7.53 (m, *J* = 8.0, 0.9 Hz, 2H), 7.45 (m, *J* = 8.2, 7.1, 1.2 Hz, 2H), 7.30 (m, *J* = 8.0, 7.1, 1.0 Hz, 2H), 4.67 (s, 4H). ^{13}C NMR (151 MHz, $CDCl_3$) δ 141.21, 128.22, 126.58, 124.43, 121.47, 119.80, 116.81, 112.39, 109.89, 77.26, 77.04, 76.83, 42.74. ESI-MS: m/z $[M+H]^+$ calculated for $C_{20}H_{15}N_2^+$: 283.12; found 283.12. HPLC: purity 99.9%.

Preparation of Polymer-Based Afterglow Films

Preparation of PVA films: PVA aqueous solution with a mass fraction of 10% and an alcoholysis degree of 72% was prepared as the host solution and a solution of **ICzO2** and **ICzC2** in THF with a concentration of 2.0 mg/mL was prepared as the guest solution. And then 5 μL, 25 μL, 50 μL, 250 μL and 500 μL of the guest solution were mixed with 1.0 g of the host solution, respectively. Subsequently, these mixtures were heated at 80 °C for 6 h after ultrasonication at 60 °C for 0.5 h, resulting in the production of PVA films doped with mass ratios of 0.01%, 0.05%, 0.10%, 0.50%, and 1.00%.

Preparation of MF films: A prepolymer of MF was prepared as the host solution from 43 g of formaldehyde aqueous solution (37%-40%) and 30.4 g of melamine and a solution of **ICzO2** and **ICzC2** in THF with a concentration of 2.0 mg/mL was prepared as the guest solution. And then 500 μL of the guest solution was mixed with 1.0 g of the host solution respectively. Subsequently, the resulting mixtures were treated in an ultrasonic bath for about 30 minutes, followed by drop-casting on quartz plates. After drying at 150 °C for 10 minutes, the MF polymer was scraped off and pressed into a translucent MF polymer film at 160 °C.

Measurements

^{1}H and ^{13}C nuclear magnetic resonance spectra of the intermediates and the final products were obtained on a Bruker AVANCE spectrometer (600 MHz) by employing $CDCl_3$ and DMSO-d_6 as solvents and tetramethylsilane as internal standard. High-resolution mass

spectrometry was carried out on the instrument of LTQ_Orbitrap_LCMS (LTQ Orbitrap Elite) to determine the exact molecular weights of the compounds. SC-XRD were recorded at about 150 K by a Bruker X-ray diffractometer (D8 ADVANCE, Germany) at a 4° (2θ)/min scan rate which copper target is used as X-ray radiation source. The crystal structures were solved directly by SHELXTL software which were refined by least square method and visualized by Olex2 and Mercury software. In addition, steady-state PL spectra, delayed emission spectra, absolute PL quantum yields, and time-resolved emission decay curves were collected using a spectrometer (FLS980) equipped with a calibrated integrating sphere and a thermostat (Oxford) from Edinburgh Instruments. The UV-Vis absorption spectroscopy (UV-VIS) were collected on a U-3900 UV spectrophotometer (Hitachi, Japan). The delayed emission spectra at 77K were collected on an Ocean Optics spectrophotometer equipped with a QE65 Pro charge-couple device (CCD) detector, a 100 mm diameter optical fiber and an optical fiber probe.

Computational details

The molecular geometries of **ICzO2** and **ICzC2** at ground state were optimized using the density functional theory (DFT) method at the B3LYP-D3(BJ)/6-311g(d) level in the Gaussian 16 program. Based on the optimized ground state geometries, **ICzO2** at S_1 state were optimized using the time-dependent density functional theory (TD-DFT) method at the B3LYP-D3(BJ)/6-311g(d) level in the Gaussian 16 program. Based on the S_1 geometries, the exciton energies in singlet (S_n) and triplet states (T_n) were estimated through a combination of TD-DFT and B3LYP-D3(BJ)/6-311g(d) level. Herein, energy levels of the possible T_n states are considered to lie within the range of $E_{S1} \pm 0.30$ eV. Based on the S_1 geometries, Spin-orbit coupling (SOC) matrix elements between the singlet and triplet excited states were calculated with spin-orbit mean-field (SOMF) methods and natural transition orbital (NTO) analysis was performed based on the TD-DFT results and subsequently visualized via GaussView (6.0.16).

Ⅱ. Typical organic blue RTP-type afterglow material at room temperature

Supplementary Table 1. Selected examples of organic blue afterglow materials with phosphorescent emission wavelength, corresponding lifetime and afterglow quantum yields under ambient conditions.

<table>
<tr>
<td> 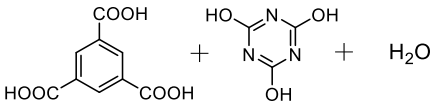
TMA CA
λ = 406 nm, τ = 1.67 s,
$\Phi_{phos.}$ = 46.1%
Nat. Commun. 2020, 11(1): 4802.</td>
<td> 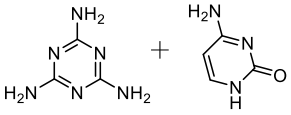
MA Ct
λ = 460 nm, τ = 0.337 s,
$\Phi_{phos.}$ = 37.11%
Adv. Opt. Mater. 2022,
10(11):2200451.</td>
<td> 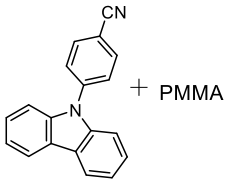
LPCN
λ = 440 nm, τ = 0.524 s,
$\Phi_{phos.}$ = 2-3%
Chem. Eng. J. 2022,
447:137458.</td>
</tr>
<tr>
<td colspan="3">1. 2. 3.
 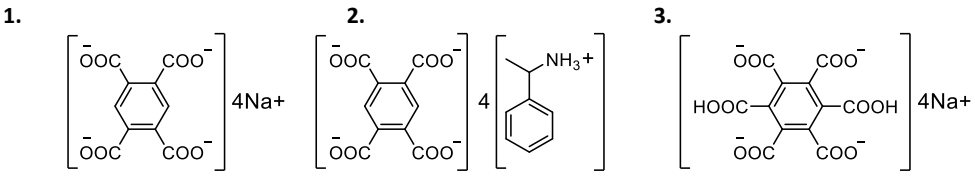
TSP TNP HSM
1. λ = 447 nm, τ = 0.178 s, $\Phi_{phos.}$ = 66.9%
2. λ = 454 nm, τ = 0.185 s, $\Phi_{phos.}$ = 96.5%
3. λ = 407 nm, τ = 0.199 s, $\Phi_{phos.}$ = 81.6%
Nat. Mater. 2021, 20(11):1539.</td>
</tr>
<tr>
<td> 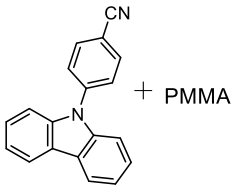
LPCN
λ = 441 nm, τ = 0.193 s,
$\Phi_{phos.}$ = 36.9%
Chem. Eng. J. 2022, 447:137458.</td>
<td> 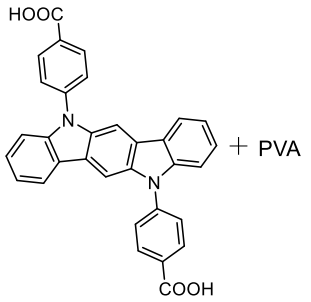
IbCzA
λ_{TADF} = 415/438 nm, τ = 1.81 s,
$\Phi_{phos.}$ = 19.8%
Angew. Chem. Int. Ed. 2022,
61(23):e202201820</td>
<td> 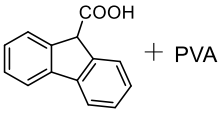
CzA
λ = 458nm, τ = 3.16 s,
$\Phi_{phos.}$ = 50%
Nat. Commun. 2022,
13(1):4890.</td>
</tr>
<tr>
<td> 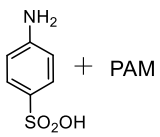
PAMABS
λ = 450 nm, τ = 0.624 s,
$\Phi_{phos.}$ = 4.08%
Chem. Eng. J. 2023, 453:139753.</td>
<td> 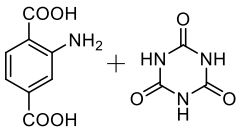
2- CA
λ = 430/460 nm, τ = 0.80 s,
$\Phi_{phos.}$ = 76.42%
Adv. Funct. Mater. 2024, 34(7):
2310198.</td>
<td> 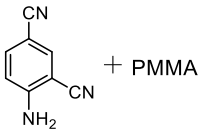
4AIN
λ = 430 nm, τ = 0.872 s,
$\Phi_{phos.}$ = 7.44%
Chem. Eng. J. 2023,
469:143929.</td>
</tr>
</table>

1.

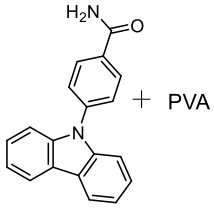

CZBM

2.

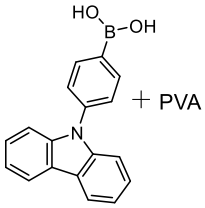

CZPA

1. λ = 435 nm, τ = 1.79 s, $\Phi_{phos.}$ = 17.8%

2. λ = 435 nm, τ = 1.97 s, $\Phi_{phos.}$ = 13.7%

Chem. Eng. J. **2023**, 452:139385.

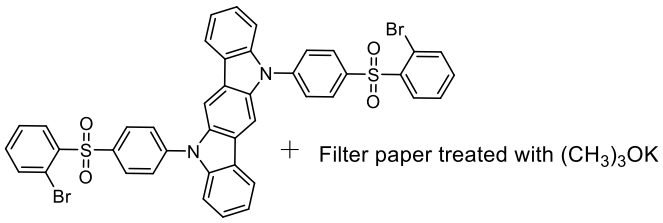

ICzS3Br

λ = 440 nm, τ = 1.07 s, $\Phi_{phos.}$ = 7.9%

J. Lumin. **2023**, 257: 119720.

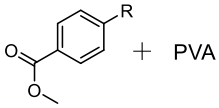

R = -$NHCH_3$ λ = 445 nm, τ = 1.926 s, $\Phi_{phos.}$ = 14.4%

R = -NH_2 λ = 440 nm, τ = 1.899 s, $\Phi_{phos.}$ = 14.2%

R = -OH λ = 415 nm, τ = 0.799 s, $\Phi_{phos.}$ = 15.4%

Angew. Chem. Int. Ed. **2024,** 63(22):e202403773.

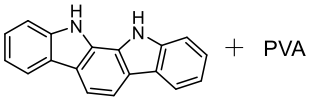

11,12-ICz

λ = 460 nm, τ = 2.04 s, $\Phi_{phos.}$ = 44.1%

Adv. Funct. Mater. **2023**, 33(1): 2208895.

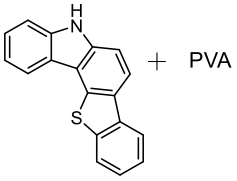

Anti-BTCz

λ = 438/460nm, τ = 0.547 s, $\Phi_{phos.}$ = 17.32%

Adv. Opt. Mater. **2024,** 12(1):2301188.

Ⅲ. Typical organic TADF-type afterglow materials at room temperature

Supplementary Table 2. Photophysical properties of the typical afterglow materials with TADF.

Sing component organic crystals

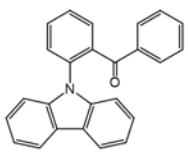

o-Cz

λ_{TADF} = 472 nm,

τ_{TADF} = 790 ms

Chem. Sci. **2019**, 10(31):7352-7.

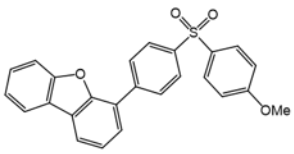

SOBF-OMe

λ_{TADF} = 476 nm,

τ_{TADF} = 204 ms

Adv. Opt. Mater. **2019**, 7(7):1801593.

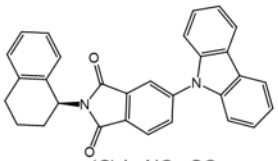

(*S*)-ImNCz-SC_p

λ_{TADF} = 500 nm,

τ_{TADF} = 464 ms

Chem. Eng. J. **2021**, 418:129167.

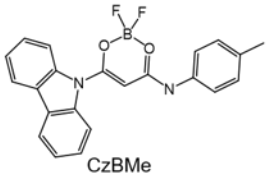

CzBMe

λ_{TADF} = 430 nm,

τ_{TADF} = 104 ms

Angew. Chem. Int. Ed. **2021**, 60(47):24984-90.

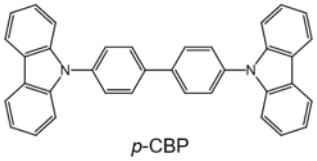

p-CBP

λ_{TADF} = 430 nm,

τ_{TADF} = 52 ms

Angew. Chem. Int. Ed. **2020**, 59(25):10032-6

Host-Guest Doping Systems based on Small Molecules

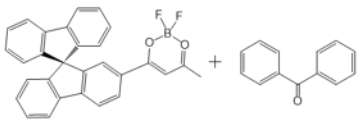

spiroBF_2-BP

λ_{TADF} = 452 nm,

τ_{TADF} = 842 ms

Adv. Opt. Mater. **2021**, 9(13):2100353

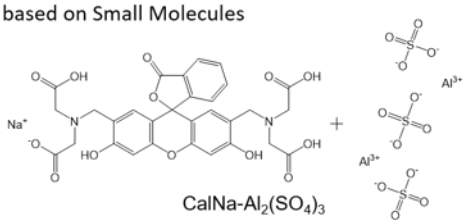

CalNa-$Al_2(SO_4)_3$

λ_{TADF} = 466 nm,

τ_{TADF} = 668 ms

Angew. Chem. Int. Ed. **2023**, 62(7): e202217616.

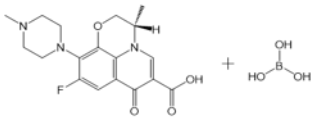

BLev

λ_{TADF} = 490 nm,

τ_{TADF} = 400 ms

Adv. Opt. Mater. **2022**, 10(18):2200629.

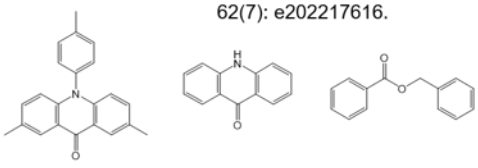

3-PhB

λ_{TADF} = 419 nm,

τ_{TADF} = 472 ms

4-PhB

λ_{TADF} = 400 nm,

τ_{TADF} = 70 ms

Chem. Mater. **2024**, 36 (6):3000

Polymer-Based Afterglow Materials

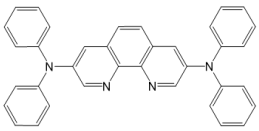

+ PMMA

PhenDpa

λ_{TADF} = 444 nm,

/

Adv. Mater. **2019**, 31(12):1807887.

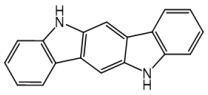

+ PMMA

ICZ-p1

λ_{TADF} = 435 nm,

τ_{TADF} = 2280 ms

Adv. Funct. Mater. **2024**, 34(37):2402428.

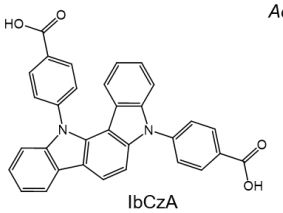

+ PVA

IbCzA

λ_{TADF} = 415 nm,

τ_{TADF} = 1810 ms

Angew. Chem. Int. Ed. **2022**, 61(23):e202201820.

.

Ⅴ. Photophysical Properties

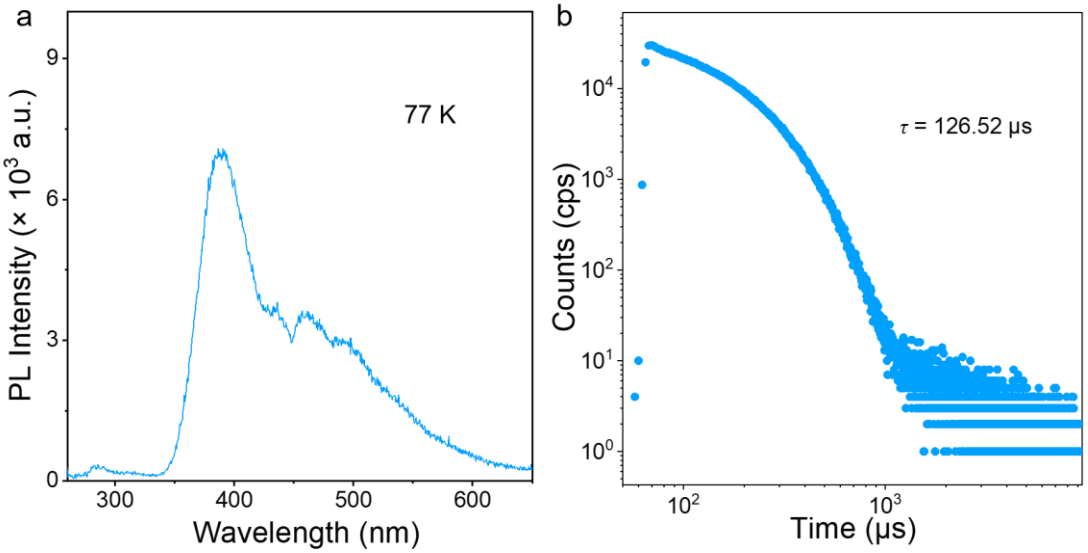

Supplementary Fig. 1 The delayed PL spectra of benzene measured at 77 K with different delay times (Excitation wavelength: 240 nm).

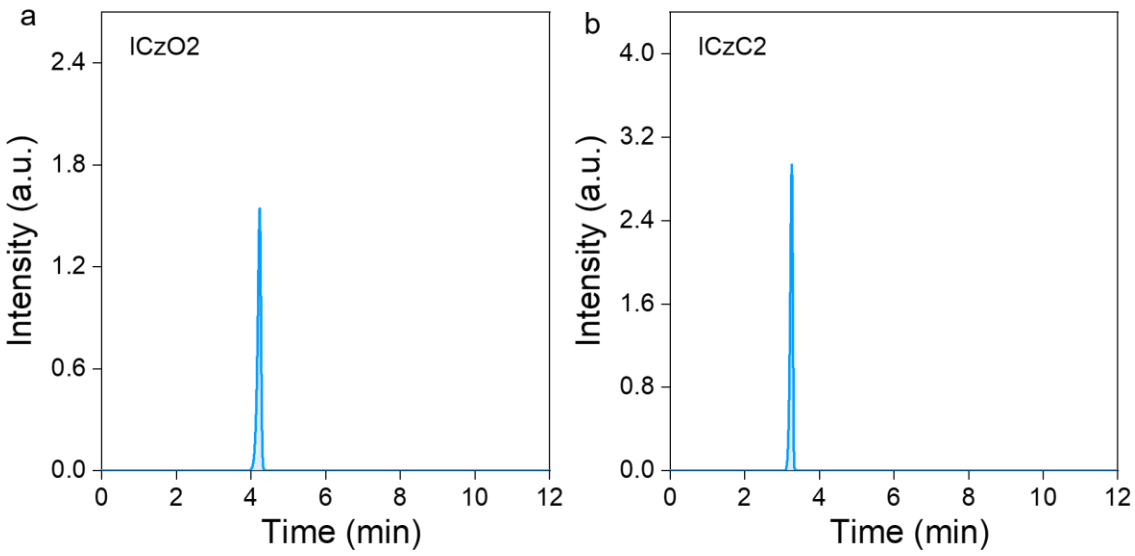

Supplementary Fig. 2 HPLC result of **ICzO2** and **ICzC2**

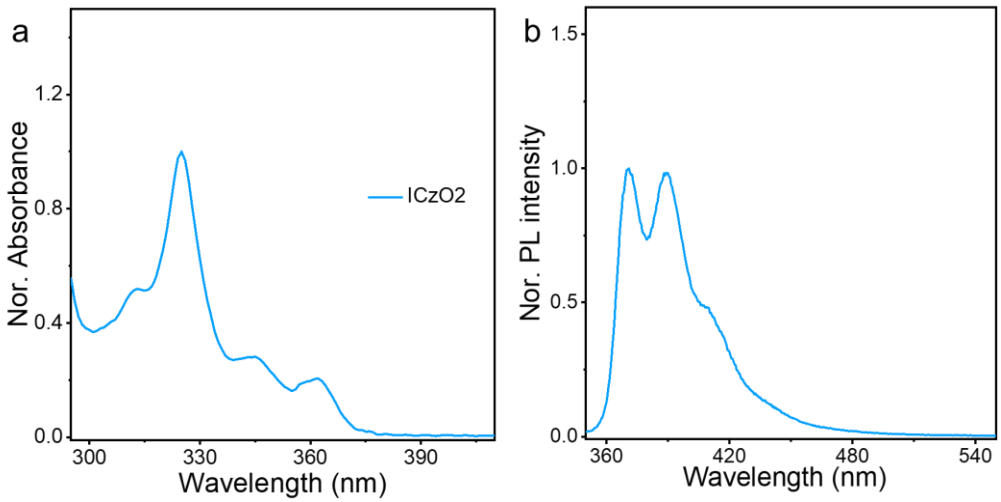

Supplementary Fig. 3 a The UV-visible absorption spectra and, **b** steady-state PL spectra of the **ICzO2** in THF ($c = 5\times10^{-5}$ M).

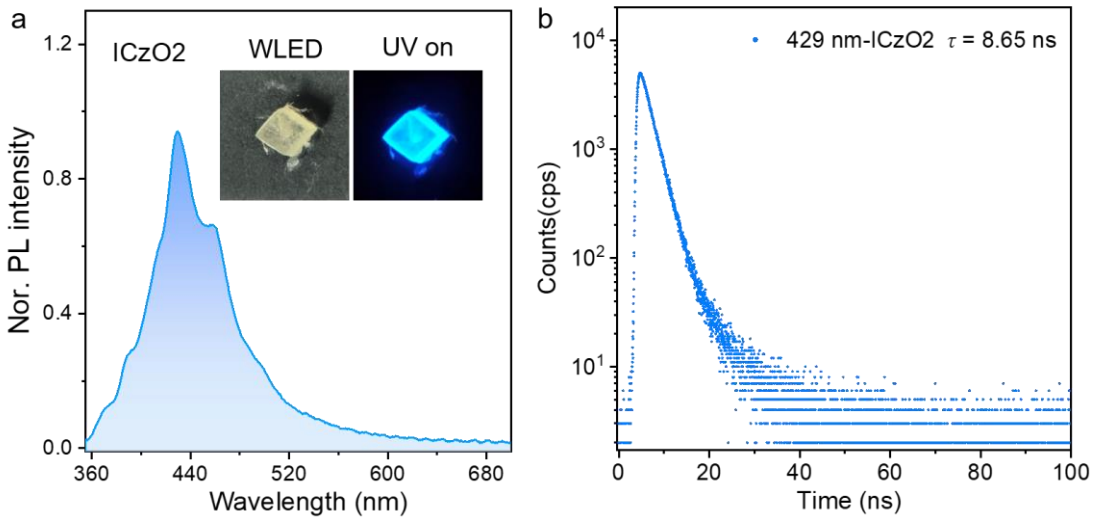

Supplementary Fig. 4 a The steady-state PL spectra and, **b** Lifetime decay profiles of the **ICzO2** crystals at ambient conditions. Insets: left, under natural light; right, under 365 nm UV irradiation.

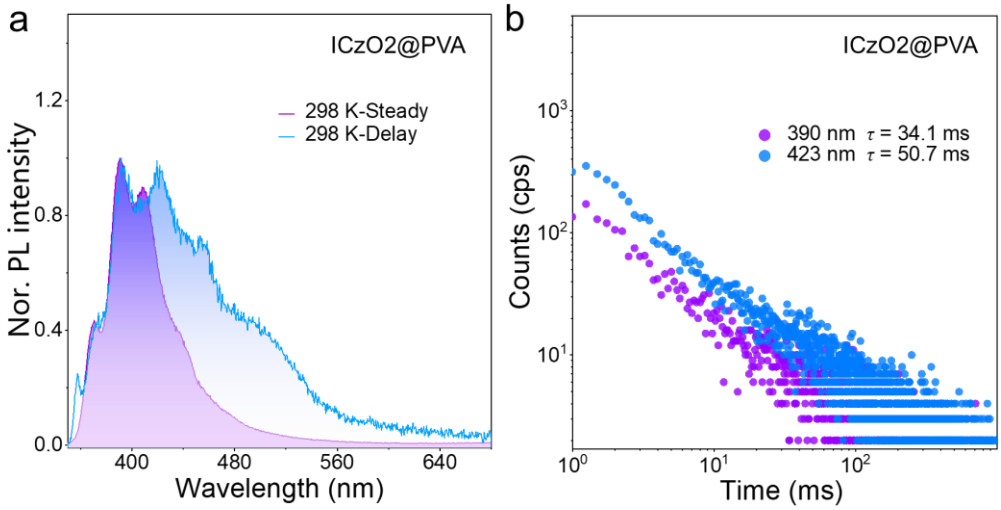

Supplementary Fig. 5 a The steady-state PL spectra and, **b** Lifetime decay profiles (Delayed 1ms) of the 0.10%-**ICzO2**@PVA before irradiation.

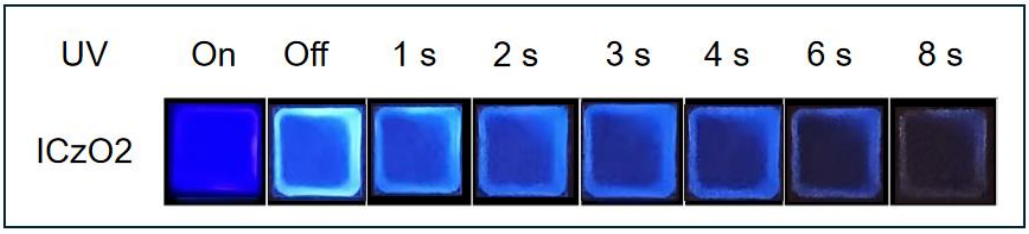

Supplementary Fig. 6 The long afterglow luminescence photos of the 0.10%-**ICzO2**@PVA after photoactivation (Excitation: 365 nm. Photoactivation: 2 min).

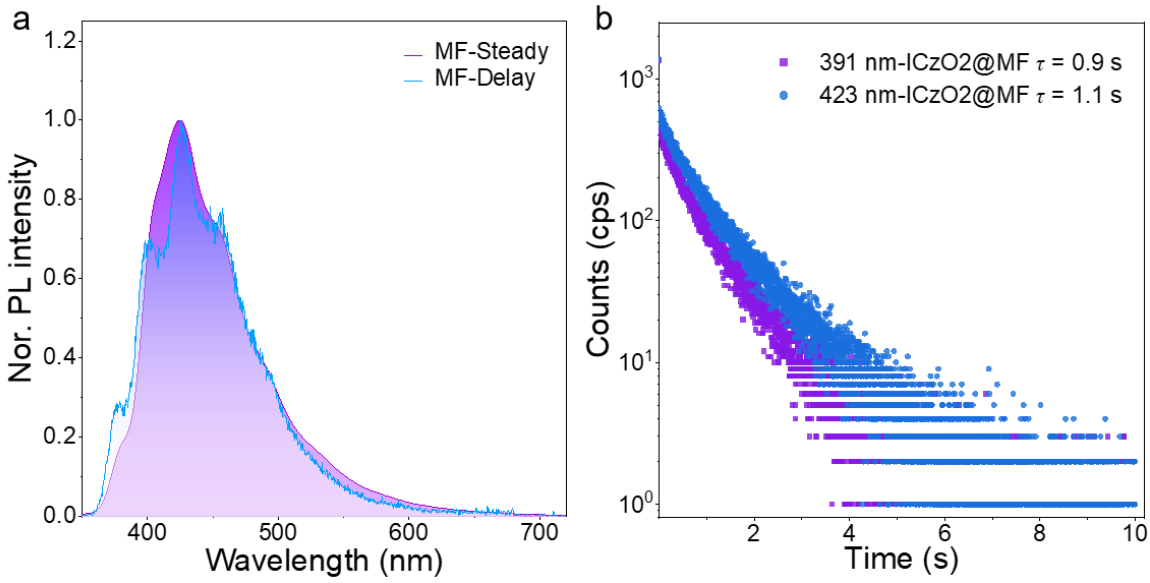

Supplementary Fig. 7 a The steady-state PL spectra and the delayed emission spectra (Delayed 1 ms) of the 0.10%-**ICzO2@MF** (Excitation: 310 nm). **b** The delayed emission decay curves and lifetimes at different emission peaks of the 0.10%-**ICzO2@MF** (Excitation: 286 nm).

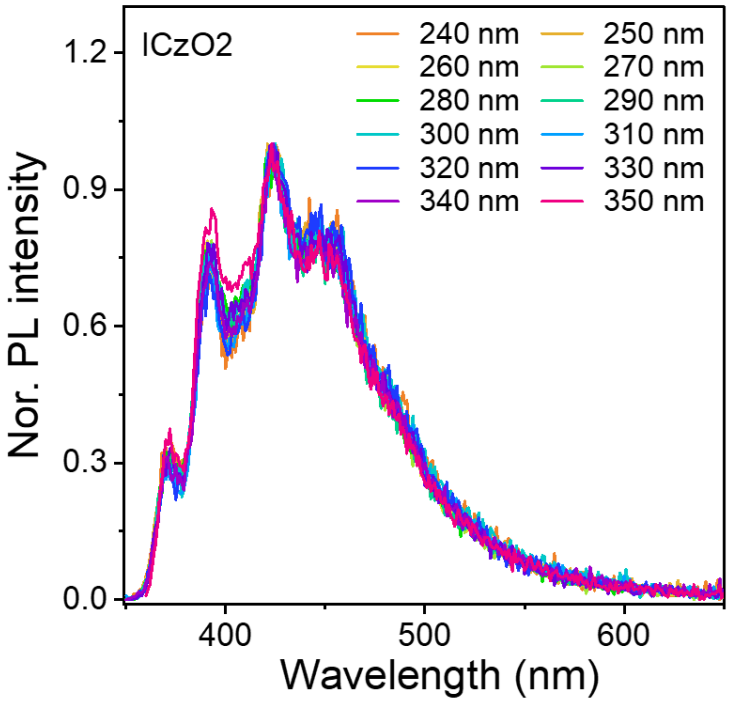

Supplementary Fig. 8 the prompt PL spectra of **ICzO2/PVA** recorded at excitation wavelengths from 250 to 400 nm.

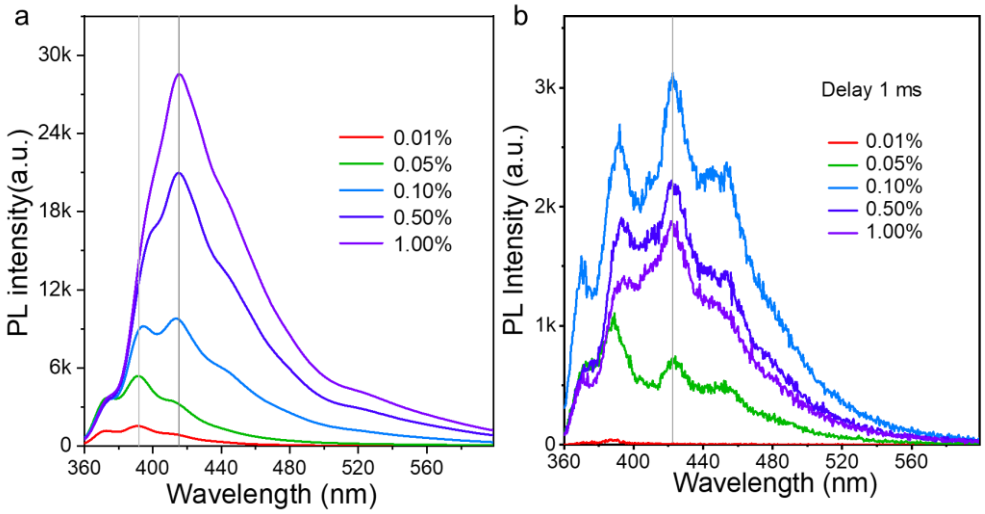

Supplementary Fig. 9 a The steady-state PL spectra and **b** the delayed PL spectra (delayed 1ms) of the **ICzO2@PVA** with different concentrations (Excitation: 310 nm).

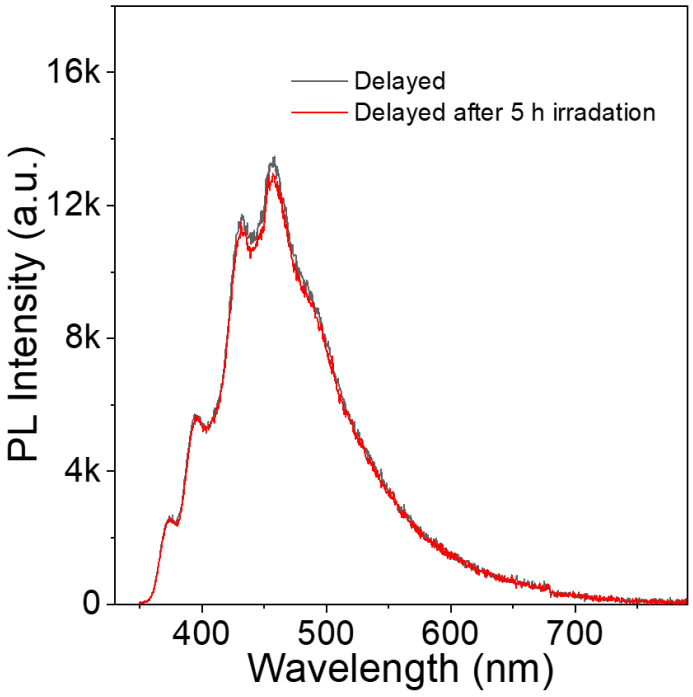

Supplementary Fig. 10 The delayed emission spectra (Delayed 1ms) after 5 h irradiation of the**ICzO2@PVA.**

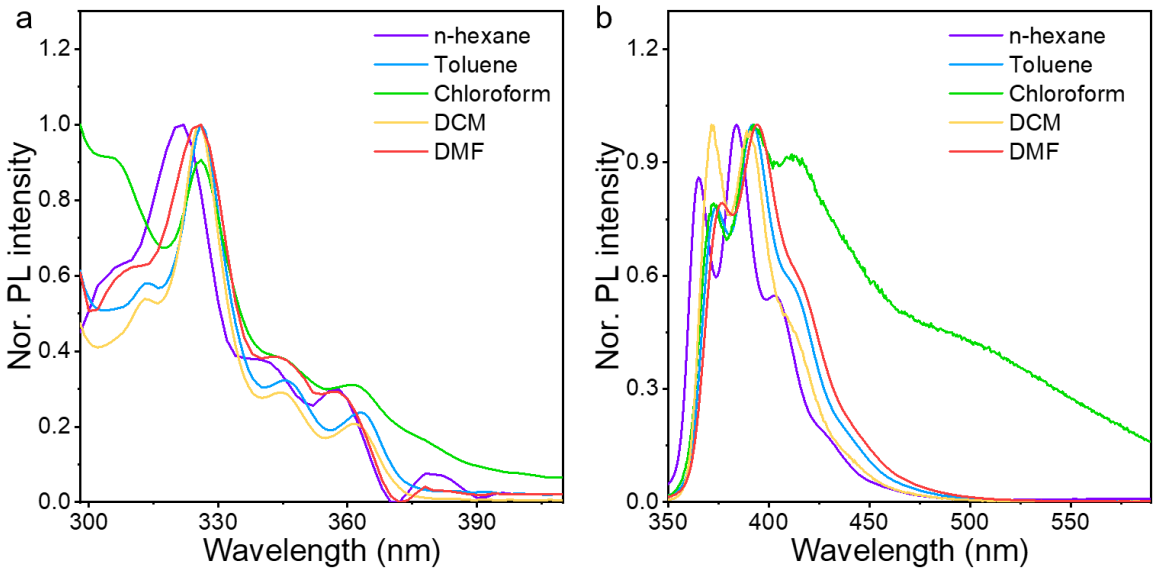

Supplementary Fig. 11 a The UV-visible absorption spectra and, **b** PL spectra of the **ICzO2** in different solvents (Molar concentration: 5×10^{-5} M).

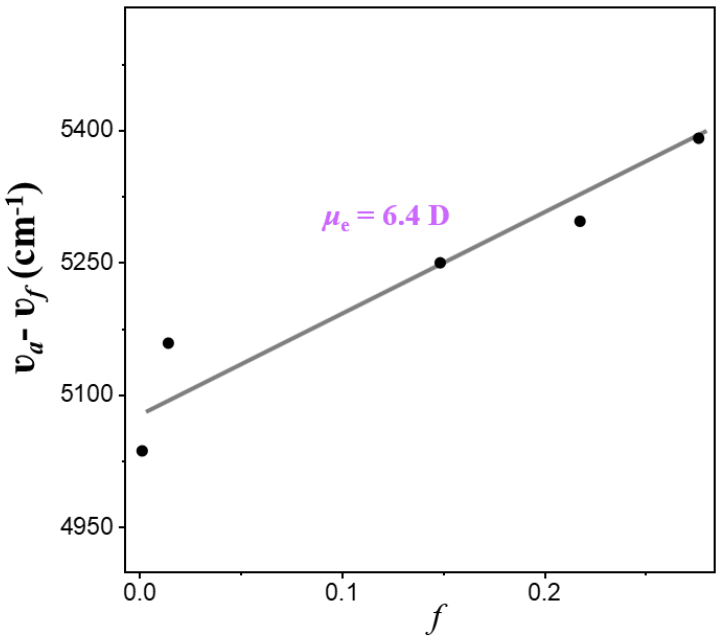

Supplementary Fig. 12 Solvation effect Lippert–Mataga models of chromophore **ICzO2**. The dots and lines refer to experimental Stokes shifts and fitting lines, respectively.

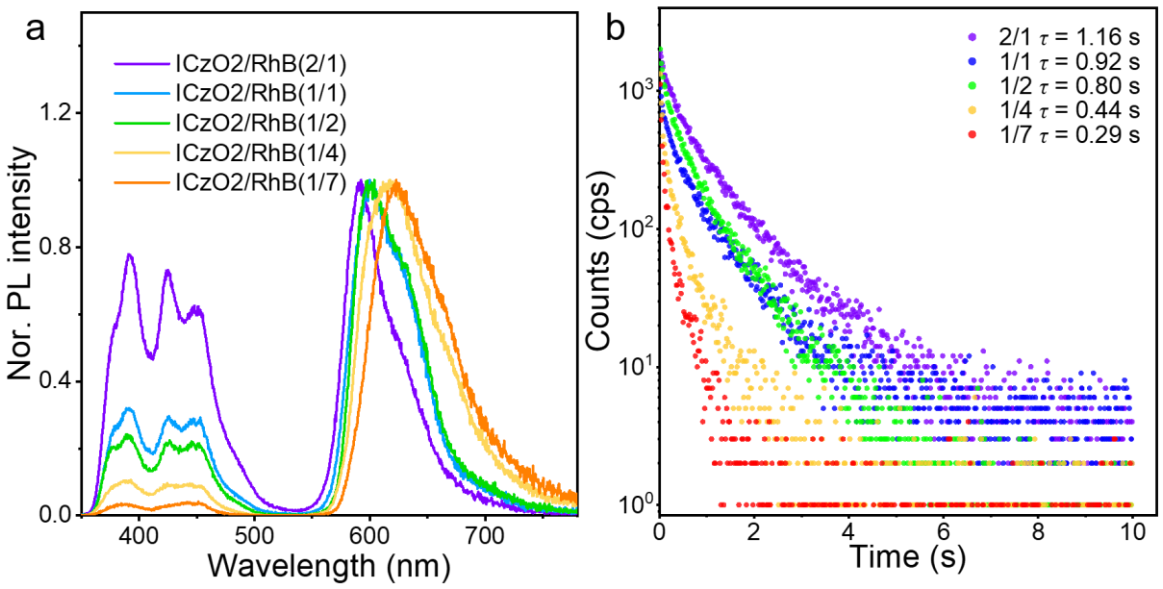

Supplementary Fig. 13 a Steady-state PL spectra and **b** lifetime decay profiles of **ICzO2/RhB** with different mixing ratios in a PVA matrix.

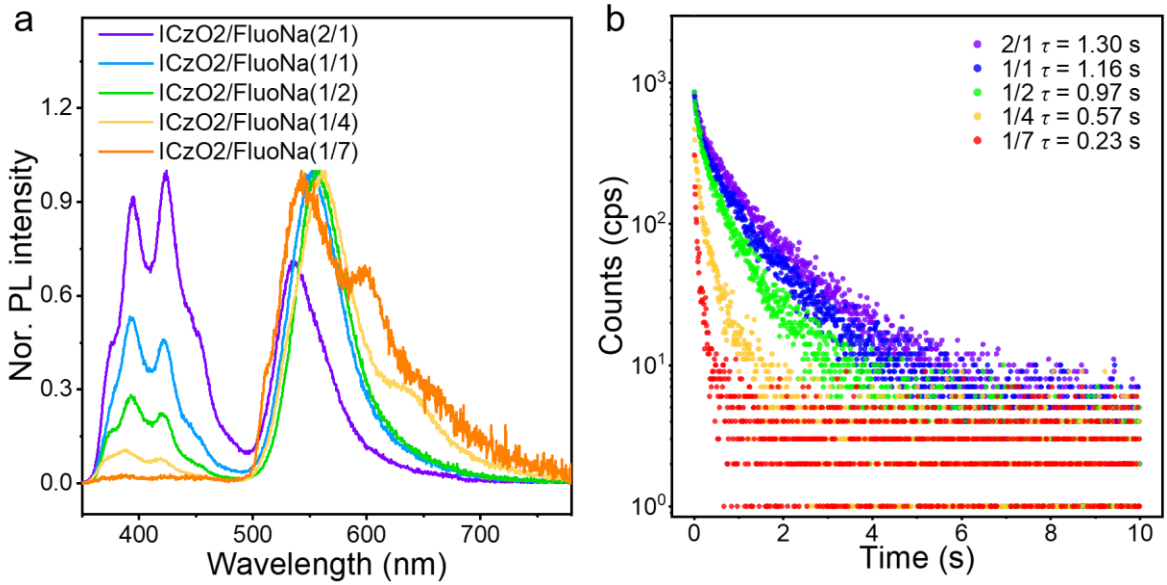

Supplementary Fig. 14 a Steady-state PL spectra and **b** lifetime decay profiles of **ICzO2/Fluona** with different mixing ratios in a PVA matrix.

VI.[1]H NMR, [13]C NMR and High-Resolution Mass Spectra Results

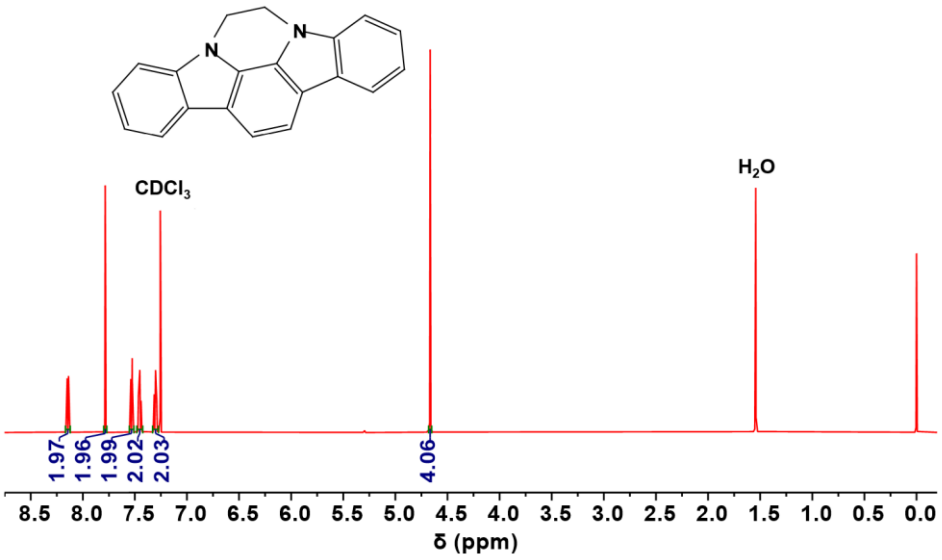

Supplementary **Fig. 14** [1]H NMR spectrum of the **ICzO2** (in $CDCl_3$).

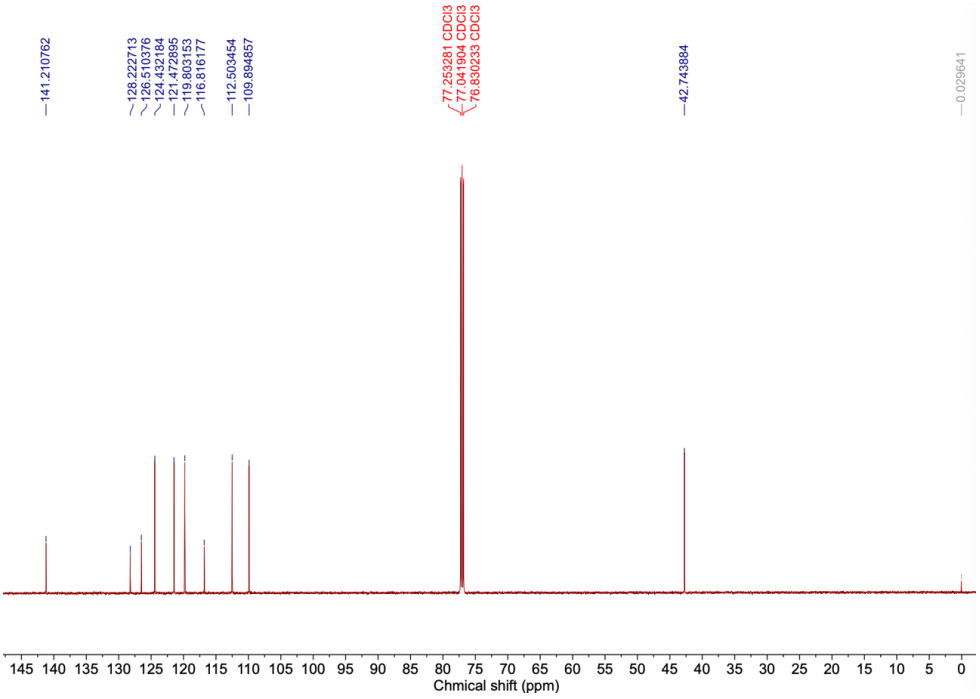

Supplementary **Fig. 15** [13]C NMR spectrum of the **ICzO2** (in $CDCl_3$).

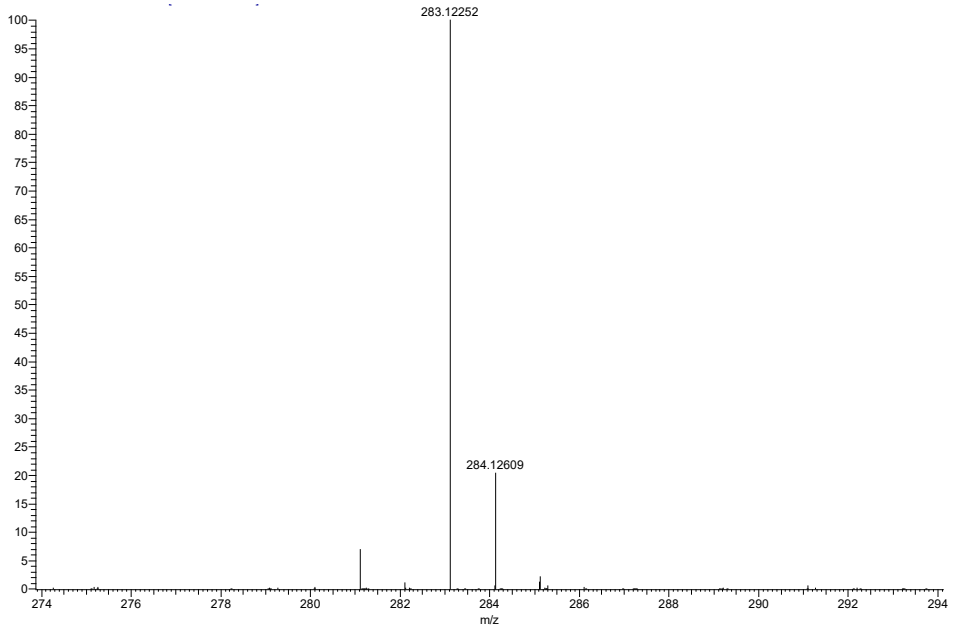

Supplementary **Fig. 16** ESI-MS spectrum of the **ICzO2**.

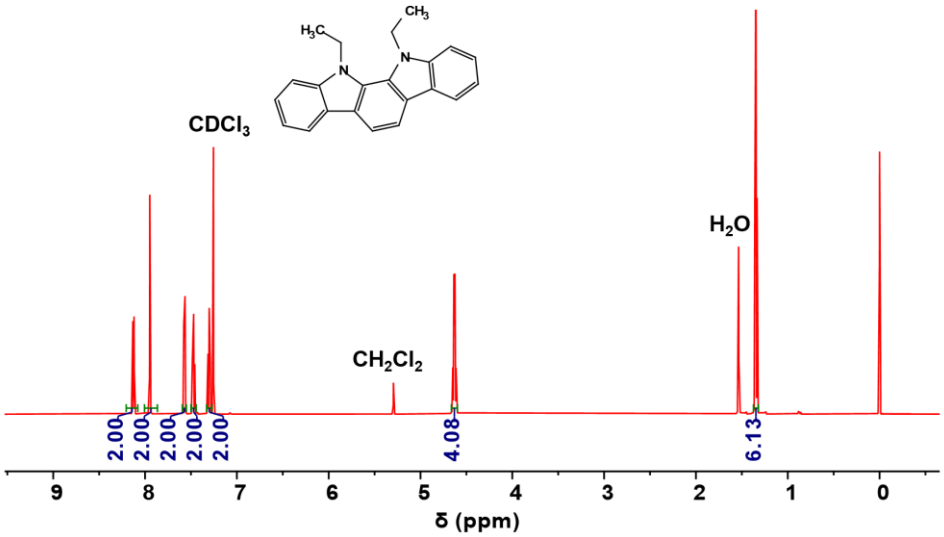

Supplementary **Fig. 17** ^{1}H NMR spectrum of the **ICzC2** (in $CDCl_3$).

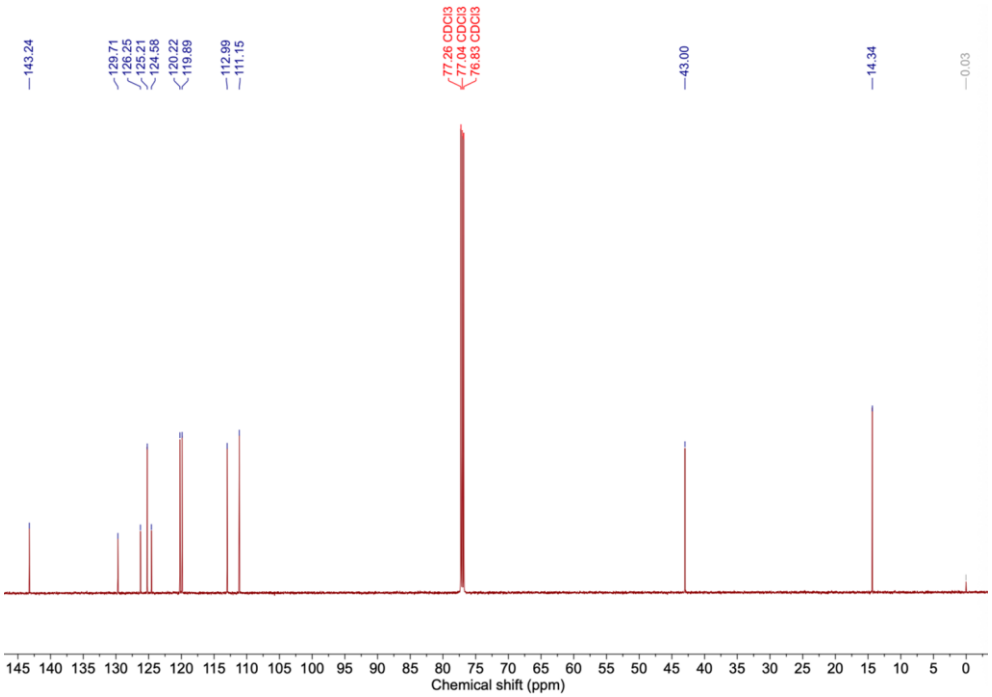

Supplementary **Fig. 18** ^{13}C NMR spectrum of the **ICzC2** (in $CDCl_3$).

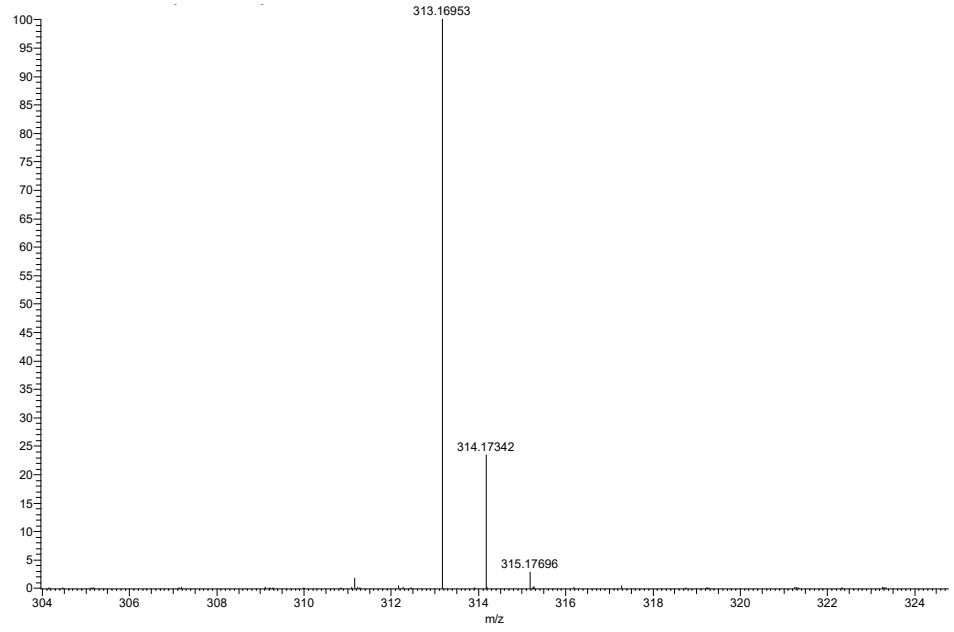

Supplementary **Fig. 19** ESI-MS spectrum of the **ICzC2**.

Supplementary **Table 3** Crystal data and structure refinement for **ICzO2** and **ICzC2**.

	ICzC2 (CCDC: 2414452)	**ICzO2** (CCDC: 2414453)
Empirical formula	$C_{22}H_{20}N_2$	$C_{20}H_{14}N_2$
Formula weight	312.4	282.33
Temperature/K	156.63(11)	155(4)
Crystal system	tetragonal	monoclinic
Space group	$I4_1/a$	$P2_1/c$
a/Å	21.8100(6)	9.0111(2)
b/Å	21.8100(6)	11.3762(3)
c/Å	13.6787(4)	13.6892(3)
α/°	90	90
β/°	90	101.355(2)
γ/°	90	90
Volume/$Å^3$	6506.7(4)	1375.84(6)
Z	16	4
$\rho_{calc}g/cm^3$	1.276	1.363
μ/mm^{-1}	0.575	0.626
F(000)	2656	592
Crystal size/mm^3	0.06 × 0.05 × 0.04	0.04 × 0.03 × 0.02
Radiation	Cu Kα (λ = 1.54184)	Cu Kα (λ = 1.54184)
2Θ range for data collection/°	7.628 to 134.02	10.012 to 134.154
Reflections collected	9973	7936
Independent reflections	2881 [R_{int} = 0.0128, R_{sigma} = 0.0113]	2454 [R_{int} = 0.0214, R_{sigma} = 0.0189]
Data/restraints/parameters	2881/0/234	2454/0/199
Goodness-of-fit on F^2	1.064	1.036
Final R indexes [I>=2σ (I)]	R_1 = 0.0320, wR_2 = 0.0827	R_1 = 0.0343, wR_2 = 0.0887
Final R indexes [all data]	R_1 = 0.0331, wR_2 = 0.0836	R_1 = 0.0359, wR_2 = 0.0898
Largest diff. peak/hole / e $Å^{-3}$	0.18/-0.13	0.14/-0.22

The change in magnitude of the dipole moment between the ground and excited states, that is, $\Delta\mu = \left|\mu_e - \mu_g\right|$ can be estimated using the Lippert–Mataga equation

$$hc\left(\upsilon_a - \upsilon_f\right) = \mathrm{hc}\left(\upsilon_a^0 - \upsilon_f^0\right) + \frac{2\left(\mu_e - \mu_g\right)^2}{a_0^3} f(\varepsilon, n)$$

Where a_0 is the cavity radius in which the solute resides, estimated to be 6.6 Å. μ_g is the ground-state dipole moment, estimated to be 3.5 D (ωB97X at the basis set level of 6-31G**), μ_e is the excited state dipole moment. h and c are Planck's constant and the speed of light, respectively, and f(ε, n)is the orientation polarizability, defined as

$$f(\varepsilon, n) = \frac{\varepsilon - 1}{2\varepsilon + 1} - \frac{n^2 - 1}{2n^2 - 1}$$

Where ε is the static dielectric constant and n is the optical refractivity index of the solvent. Through the analysis of the fitted line in low-polarity solvents, its corresponding μ_e was calculated to be 6.4 D with the slope of 908.4 (r^2= 0.9115) according to Lippert-Mataga equation

Supplementary Table 4 Photophysical parameters of emitters (4CzIPN and ICzO2) in different solvents

Solvents	ε	n	$f(\varepsilon, n)$	ν_a-ν_f (cm^{-1})	
				4CzIPN	ICzO2
Hexane	1.9	1.375	0.001225	2078.51	5037
Toluene	2.38	1.494	0.014104	2690.97	5159
Chloroform	4.81	1.446	0.14823	2942.46	5250
DCM	8.93	1.424	0.21717	3741.54	5297
DMF	37	1.427	0.275703	5111.20	5391

Supplementary Table 5 Energy diagram of the first four singlet and triplet excited states of ICzO2 obtained from TD-M06-2X calculations. f represents the oscillator strength.

Excited State	Energy Level [eV]	f	Transition Configuration [%]	SOC Constant [cm^{-1}]	
ICzoO2					
S_1	3.5129	0.04440	H -> L 95.4%		
S_2	4.0763	0.13890	H-1 -> L 60.3%, H -> L+1 32.7%		
S_3	4.3673	0.24870	H -> L+1 56.6%, H -> L+2 21.2%		
S_4	4.6303	0.00050	H-2 -> L 88.3%, H-1 -> L+3 6.3%		
T_1	2.9083		H -> L 95.1%	S_0	0.29698
				S_1	0.01414
T_2	3.0916		H-1 -> L 75.4%, H -> L+2 6.1%	S_1	0.05196
T_3	3.4930		H -> L+1 76.8%, H-2 -> L 6.6%	S_1	0.18627
T_4	3.7325		H-1 -> L+1 47.0%, H-3 -> L 19.2%	S_1	0.08485
T_5	3.9140		H-2 -> L 44.4%, H -> L+2 27.7%	S_1	0.05830

Notes： the S_1 and T_1 energy levels derived from the fluorescence and phosphorescence spectra are 3.48 and 2.85 eV, respectively, in good agreement with the calculated values of 3.51 and 2.91 eV. The calculated S_1–T_1 energy gap, ΔE_{ST}, is 0.60 eV, close to the experimental value of 0.63 eV. Although the T_2 energy level cannot be directly determined experimentally, the excellent agreement between theory and experiment for S1 and T1 supports the reliability of the calculated excited-state energies. Thus, the calculated S_1–T_2 energy gap of 0.42 eV can be regarded as a reasonable estimate.

VII. References

[1] M.J. Frisch, G.W. Trucks, H.B. Schlegel, G.E. Scuseria, M.A. Robb, J.R. Cheeseman, G. Scalmani, V. Barone, G.A. Petersson, H. Nakatsuji, X. Li, M. Caricato, A.V. Marenich, J. Bloino, B.G. Janesko, R. Gomperts, B. Mennucci, H.P. Hratchian, J.V. Ortiz, A.F. Izmaylov, J.L. Sonnenberg, Williams, F. Ding, F. Lipparini, F. Egidi, J. Goings, B. Peng, A. Petrone, T. Henderson, D. Ranasinghe, V.G. Zakrzewski, J. Gao, N. Rega, G. Zheng, W. Liang, M. Hada, M. Ehara, K. Toyota, R. Fukuda, J. Hasegawa, M. Ishida, T. Nakajima, Y. Honda, O. Kitao, H. Nakai, T. Vreven, K. Throssell, J.A. Montgomery Jr., J.E. Peralta, F. Ogliaro, M.J. Bearpark, J.J. Heyd, E.N. Brothers, K.N. Kudin, V.N. Staroverov, T.A. Keith, R. Kobayashi, J. Normand, K. Raghavachari, A.P. Rendell, J.C. Burant, S.S. Iyengar, J. Tomasi, M. Cossi, J.M. Millam, M. Klene, C. Adamo, R. Cammi, J.W. Ochterski, R.L. Martin, K. Morokuma, O. Farkas, J.B. Foresman, D.J. Fox, Gaussian 09 Rev. D.01, in, Wallingford, CT, 2013.

[2] Z. An, C. Zheng, Y. Tao, R. Chen, H. Shi, T. Chen, Z. Wang, H. Li, R. Deng, X. Liu, W. Huang, Stabilizing triplet excited states for ultralong organic phosphorescence, Nat. Mater., 14 (2015) 685-690.